Dynamics of Atmospheres and Oceans 108 (2024) 101504

Contents lists available at ScienceDirect

Dynamics of Atmospheres and Oceans

journal homepage: www.elsevier.com/locate/dynatmoce

The curious case of a strong relationship between ENSO and Indian summer monsoon in CFSv2 model

Priyanshi Singhai [a,b,c,*], Arindam Chakraborty [a,b], Kaushik Jana [d], Kavirajan Rajendran [e,f], Sajani Surendran [f], Kathy Pegion [c]

[a] Centre for Atmospheric and Oceanic Sciences, Indian Institute of Science, CV Raman Rd, Bengaluru, 560012, Karnataka, India
[b] Divecha Centre for Climate Change, Indian Institute of Science, CV Raman Rd, Bengaluru, 560012, Karnataka, India
[c] School of Meteorology, University of Oklahoma, 120 David L Boren Blvd, Norman, 73072, OK, USA
[d] Mathematical and Physical Sciences Division, Ahmedabad University, Commerce Six Roads, Naranpark Society, Navrangpura, Ahmedabad, 380009, Gujarat, India
[e] Kerala State Council for Science, Technology and Environment (KSCSTE), Institute for Climate Change Studies (KSCSTE-ICCS), Deepthi Nagar Road Kanjikuzhi, Kottayam, 686004, Kerala, India
[f] CSIR Fourth Paradigm Institute (CSIR-4PI), NAL Belur Campus Wind Tunnel Road, Bengaluru, 560037, Karnataka, India

ARTICLE INFO

Keywords:
Ensemble mean
ENSO
Indian summer monsoon
Teleconnection
CFSv2

ABSTRACT

An ensemble of forecasts is necessary to identify the uncertainty in predicting a non-linear system like climate. While ensemble averages are often used to represent the mean state and diagnose physical mechanisms, they can lead to information loss and inaccurate assessment of the model's characteristics. Here, we highlight an intriguing case in the seasonal hindcasts of the Climate Forecast System version 2 (CFSv2). While all ensemble members often agree on the sign of predicted El Niño Southern Oscillation (ENSO) for a particular season, non-ENSO climate forcings, although present in some of the individual members, are disparate. As a result, an ensemble mean retains ENSO anomalies while diminishing non-ENSO signals. This difference between ENSO and non-ENSO signals significantly influences moisture convergence and Indian summer monsoon rainfall (ISMR). This stronger influence of ENSO on seasonal predictions increases ENSO–ISMR correlation in ensemble mean seasonal hindcasts. Thus, this discrepancy in the ENSO–ISMR relationship is not present in the individual ensemble members, considered individually or together (without averaging) as independent realizations. Therefore, adequate care should be taken while evaluating physical mechanisms of teleconnection in ensemble mean predictions that can often be skewed due to constructive or destructive superposition of different impacts.

1. Introduction

Ensemble forecasting has become widely adopted for predicting inherently chaotic and non-linear systems like weather and climate (Molteni et al., 1996; Palmer, 2000). This approach involves running a numerical prediction model multiple times with different initial conditions or numerical atmospheric representations to address forecast uncertainty (Palmer, 2000; Leutbecher and Palmer, 2008; Weisheimer et al., 2011). Moreover, ensemble averages of forecasts are commonly used to address systematic model errors, quantify forecast uncertainty, and represent forecasts as anomalies. It is commonly (Toth and Kalnay, 1997; Hamill and Colucci, 1997; Du et al., 1997; Ebert, 2001; Krishnamurti et al., 1999; Casanova and Ahrens, 2009; Singhai et al., 2020; Surcel et al.,

* Corresponding author at: School of Meteorology, University of Oklahoma, 120 David L Boren Blvd, Norman, 73072, OK, USA.
E-mail address: priyanshi.singhai-1@ou.edu (P. Singhai).

https://doi.org/10.1016/j.dynatmoce.2024.101504
Received 11 April 2024; Received in revised form 19 October 2024; Accepted 26 October 2024
Available online 2 November 2024
0377-0265/© 2024 Elsevier B.V. All rights are reserved, including those for text and data mining, AI training, and similar technologies.

2014) that the ensemble average/mean tends to outperform the majority or all of the individual ensemble members. Christiansen (2018) attributed this difference to non-intuitive properties of high-dimensional spaces, such as the curse of dimensionality, and demonstrated why the error of the ensemble mean is typically around 30% less than the typical error of individual ensemble members (Gleckler et al., 2008; Sillmann et al., 2013; Flato et al., 2014).

The superiority of ensemble mean over individual ensemble members is attributed to the cancellation of random errors across members and providing a better estimate of non-linear diagnostic quantities (Hagedorn et al., 2005) through non-linear filtering effect (Toth and Kalnay, 1997; Surcel et al., 2014). The ensemble mean approach relies on the forecast value for a specific start time, lead time, and target period (Christiansen, 2019). However, there can be challenges if a forecast ensemble mean is needed for start times that are not included in the hindcasts or if the number of hindcasts is considerably smaller than the variance of the forecast anomaly (Tippett et al., 2018). Despite these challenges, numerous studies have extensively utilized this method to evaluate the model's teleconnection patterns and forecast skill in simulating Indian summer monsoon rainfall (ISMR) (Kim et al., 2012; George et al., 2016; Chattopadhyay et al., 2016; Attada et al., 2022; Ehsan and Singh, 2023; Singh et al., 2024).

The year-to-year variation of ISMR is primarily influenced by low-frequency variations in tropical sea surface temperatures (Charney and Shukla, 1981), particularly related to El Niño Southern Oscillation (ENSO) (Rasmusson and Carpenter, 1983; Shukla and Wallace, 1983). However, the impact of these SST variations on monsoons can vary due to the inherent chaotic nature of the climate system. Hence, ensemble forecasts become imperative to estimate the uncertainty associated with the ISMR predictions and to evaluate the model performance in predicting monsoons. Many climate models participating in phases 1 and 2 of the North American Multi-Model Ensemble (NMME), heavily rely on ENSO for predicting ISMR. Notably, some models in the NMME exhibit an ENSO–ISMR relationship nearly twice as strong as observed (Singh et al., 2019). A study by Ramu et al. (2018) has shown that many models of Coupled Model Intercomparison Project Phase 5 (CMIP5) show that the displacement of key circulation patterns, including the anticyclone in the southeastern Indian Ocean and the cyclone in the western subtropical North Pacific, results in greater advection of dry winds from West Asia towards the Indian subcontinent. Additionally, the models simulate stronger upper-level convergence and lower-level divergence, which intensifies the suppression of the Indian monsoon during El Niño events. The National Centers for Environmental Prediction (NCEP) Climate Forecast system version-2 (CFSv2) model overestimates this relationship (George et al., 2016; Chattopadhyay et al., 2016), potentially due to an underestimation of synoptic activity over the Bay of Bengal in August, which amplifies the impact of ENSO on ISMR in the model (Das et al., 2022). Furthermore, the ENSO–ISMR relationship in the CFSv2 might also be influenced by SST biases in the equatorial central Pacific and Indian oceans (Shukla and Huang, 2016). (Krishnamurthy, 2018) suggested that the CFSv2 model has a problem capturing the air-sea interaction over the Indian Ocean and low-level winds over the Indian region. Sabeerali et al. (2019) shows that CFSv2 has poor predictive skills in forecasting the teleconnection between the Atlantic zonal mode and ISM.

Previous studies have highlighted that in CFSv2, ISMR variability is primarily determined by ENSO, whereas in observations, other factors (such as Indian Ocean Dipole (IOD) and Atlantic Tropical Variability (ATL)) also play significant roles (Kim et al., 2012; Shukla and Huang, 2016; He et al., 2022; Rajendran et al., 2021; Behera et al., 1999; Ashok et al., 2001; Kucharski et al., 2007; Sabeerali et al., 2019). However, in our previous work (Singhai et al., 2023), we noted an interesting observation that El Niño related droughts in the CFSv2 model represent only one-third of occurrences, while in observations, they make up two-thirds. This observation prompted us to investigate the ENSO–ISMR relationship further. Since numerous previous studies analyzed the model's teleconnection patterns using the ensemble average of the forecast (Kim et al., 2012; Shukla and Huang, 2016; He et al., 2022; Rajendran et al., 2021), relying solely on this approach could lead to the loss of valuable information embedded within the individual ensemble forecasts. A study by Christiansen (2019) highlights that there is a tendency for the ensemble mean to converge towards the median error of all ensemble members, indicating that it may not fully capture the variability and valuable information present in individual forecasts. Moreover, the study also shows that, for certain lead times, the ensemble mean approach might result in a loss of important details contained within the individual forecasts, especially in regions with high variability. Hence, the primary focus of this study is to evaluate whether using the ensemble mean approach accurately captures the model's behavior in simulating ISMR teleconnection patterns. Instead of analyzing each ensemble member individually, we have chosen to consider all ensemble members collectively to better represent the model's teleconnection patterns. Additionally, we aim to identify any differences in the ensemble mean characteristics when assessing the ENSO–ISMR relationship, compared to analyzing all ensemble members together.

2. Model description, experimental design, and observational data sets

We utilize the NCEP CFSv2 model, a fully coupled system. It comprises the NCEP Global forecast system model with triangular truncation at 126 waves and 64 vertical levels, coupled to the Geophysical Fluid Dynamics Laboratory Modular Ocean Model version 4, the four-layer Noah land surface model, and the two-layer sea ice model (Saha et al., 2014). The horizontal resolution in grid space is equivalent to 0.91°. The model simulation is performed at the computing platform of Council for Scientific and Industrial Research (CSIR) Fourth Paradigm Institute, Bengaluru, following the experimental setup used by Rajendran et al. (2021), Singhai et al. (2023). The model is integrated for nine months using five different initial conditions (ICs) for the period of 1979–2016. The initial conditions include 00UTC of 21 April (member 1), 26 April (member 2), 1 May (member 3), 6 May (member 4), and 11 May (member 5). This is referred to as "Model 1" or M1 in this study. These initial conditions are chosen because we intend to consider late April/early May initial conditions, as these have been shown to provide the highest ISMR forecast skill for the CFSv2 model (Rajendran et al., 2021; Pillai et al., 2022). Given the limited number of initial conditions available for model M1, we validate its results by comparing them with those of "Model M2" or M2, which comprises 124 ensemble members initialized every fifth day

from 1 January to 31 May. These M2 ensemble members are initialized from CFS-based initial conditions and cover the period from 1982 to 2010, with four reforecasts per day (00, 06, 12, 18 UTC) as documented by Saha et al. (2010).

In order to determine the difference in characteristics between the ensemble mean and the model's actual behavior, we treat each ensemble member as a distinct entity and aggregate them together to form AM ("All Members"). AM is defined as the set of all ensemble members. Here, we have integrated five ensemble members of model M1 for the period of 1979–2016 (38 years). Therefore, AM consists of 190 years of data obtained by combining 38 years of data from five ensemble members (38 years × 5 ensemble members). A mathematical expression of the AM for any variable (like ISMR, ENSO, or the ATL index) is provided below:

$$\text{AM} = \{Var_{i,j} \mid i = 1, \ldots, 5 \text{ (IC per year)},\ j = 1, \ldots, 38 \text{ (years)}\}$$

where the index i represents the initial condition and j represents the years.

EM represents the ensemble mean, calculated by averaging the variable across all ensemble members (m).

$$\text{EM} = \frac{1}{M}\sum_{m=1}^{M} Var_m$$

The anomalies for each ensemble member are calculated by subtracting the respective climatology of each ensemble member. It is noted that the climatological mean is the same for both EM and AM, derived as the average of the values of a variable from 1979 to 2016 for each ensemble member individually (Supplementary Figure 1).

The ISMR (P) for any member m can be written as a linear combination of various SST (T) variabilities, such as ENSO, IOD, and ATL, as follows:

$$P_m = C_{0m} + \sum_{f=1}^{F} C_{fm} T_{fm} \tag{1}$$

where T_{fm} is the fth SST forcing (such as ENSO, IOD, ATL indices). C_{fm} are regression constants that measure the relative contributions of different SST variability to precipitation. The term C_{0m} can be neglected by removing the climatological mean from each ensemble member.

If there are M members in an ensemble prediction system, the above-mentioned equation is applicable individually to each ensemble member to calculate the simulated ISMR of that member. Thus, EM precipitation can be written as:

$$\bar{P} = \frac{1}{M}\sum_{m=1}^{M} P_m \tag{2}$$

By substituting the value P_m from Eq. (1) into Eq. (2), we obtain

$$\bar{P} = \frac{1}{M}\sum_{m=1}^{M}\sum_{f=1}^{F} C_{fm} T_{fm} \tag{3}$$

$$= \sum_{f=1}^{F}\left[\bar{C}_f \quad \frac{1}{M}\sum_{m=1}^{M} T_{fm}\right], \tag{4}$$

where $\bar{C}_f$ represents the 'mean' coefficient for the forcing f and is assumed to be independent of the ensemble member m. This assumption is valid as we are averaging over the same model's ensemble members with similar characteristics of different forcings across simulations. Thus, the ensemble mean (EM) ISMR represents the combined effect of the mean SST forcing derived from each ensemble member and can be computed as follows.

$$\bar{P} = \sum_{f=1}^{F} \bar{C}_f \bar{T}_f \tag{5}$$

where $\bar{T}_f$ represents the ensemble mean SST forcing.

$$\bar{T}_f = \frac{1}{M}\sum_{m=1}^{M} T_{fm}$$

The behavior of the ensemble mean value of ISMR ($\bar{P}$) may vary significantly from the actual ISMR behavior of the model. This discrepancy arises because $\bar{P}$ is influenced by the mean SST forcings ($\bar{T}_f$) rather than the actual SST forcing inherent in all ensemble members (T_f), which is accountable for the interannual variation of ISMR. We will delve deeper into this in the results section.

For comparing model results against observations, we use the June–September (JJAS) averaged Extended reconstructed sea surface temperature ERSST version 5 data (Huang et al., 2017) to calculate the ENSO and ATL index. The India Meteorological Department (IMD) monthly mean gridded rainfall dataset with a spatial resolution of 1° × 1° is used to calculate ISMR index (Rajeevan et al., 2006). JJAS average Global Precipitation Climatology Project (GPCP) data is also utilized to depict changes in precipitation over land and ocean (Huffman et al., 2009).

Index calculation

The area-averaged rainfall over the region (7.5°–27.5° N, 70°–90° E) during the boreal summer monsoon season is used to define ISMR (Parthasarathy et al., 1994). For ISMR computation, only land grid points are considered. The ENSO index is the area-average SST anomaly over the Niño 3.4 region (5° S–5° N, 170° W–120° W). SST anomaly greater (less) than 0.5 °C (−0.5 °C) is classified as El Niño (La Niña). The ATL is defined as the averaged SST anomaly over a region (20° S–Eq, 30° W–20° E) (Kucharski et al., 2008, 2007). The positive (negative) phases of ATL are identified when the JJAS averaged values exceed one (less than minus one) standard deviation. The relationship between these variables may vary depending on the dataset and time-period used (Cash et al., 2015; Ehsan et al., 2023).

Likelihood histogram

The likelihood histogram displays the distribution of ensemble members exhibiting coherent behavior, with a threshold of 0 °C for both the ENSO and ATL indices. For a particular year, we determine the maximum number of ensemble members showing the same sign of anomaly (>0 or <0). For instance, years where all five ensemble members showed either a positive or negative ENSO index are grouped in bin 5, while the 4 and 3 contained years with fewer coherent members.

3. Results

ENSO has a strong relationship with ISMR, with a correlation coefficient of −0.58, as shown in Fig. 1a. However, the majority of the climate models, including CFSv2, overestimate the impact of ENSO on boreal summer monsoon rainfall, as reported in previous studies (Kim et al., 2012; Shukla and Huang, 2016; He et al., 2022; Rajendran et al., 2022). These studies often use the ensemble mean method to examine the teleconnection patterns in the seasonal and sub-seasonal prediction systems. Although this method effectively reduces the random variations or "noise" inherent in ensemble forecasts, it also results in the loss of important information embedded in individual ensemble members.

Fig. 1a also shows the correlation coefficient (CC) between ENSO and ISMR examined in model M1 and M2 through two approaches: ensemble mean (EM, red bars) and combining all members together (AM, yellow bars). This comparison aims to discern the contrasting characteristics of both methods for Model 1 (M1) with 5 ensemble members and Model 2 (M2) with 124 ensemble members. It is important to highlight that there is a significant difference in the ENSO–ISMR relationship computed from these two methods for both models, M1 and M2. For instance, it is worth noting that the correlation coefficient calculated by combining all members, AM ($CC_{M1} = -0.55$ and $CC_{M2} = -0.58$) is comparable to that seen in the observation (CC = −0.58). However, the relationship is greatly overestimated for the ensemble mean approach, EM, resulting in a notably high correlation coefficient of −0.7 for model M1 and −0.88 for model M2. Using the t-test, the correlation coefficients of models M1 and M2 for AM and EM are different at the 95% significance levels. Moreover, the difference in the correlation coefficient between EM and AM is more pronounced for model M2, which features a considerably greater number of ensemble members compared to model M1. This indicates that the characteristics of the ENSO–ISMR relationship in the ensemble mean (EM) significantly differ from those when all members are taken into account (AM). In addition, our primary finding concerning the difference in the ENSO–ISMR relationship between the EM and AM methods remains robust and consistent regardless of the number of ensemble members used in models M1 and M2. This highlights the robustness of our results despite the potential impact of the number of ensemble members on the efficacy of the ensemble average method.

Fig. 1b–i displays the spatial patterns showing the response of ENSO to ISMR for observation (Fig. 1b), all members together (AM, Fig. 1c), ensemble mean (EM, Fig. 1d), and the individual ensemble members of model M1 (Fig. 1e–i). Negative correlation coefficient values mark the entire Indian region in all three cases. However, these values are significantly higher for the ensemble mean than for observation, all members, and individual ensemble members. Moreover, the AM values appear to be similar to the observations, particularly over the Western Ghats. The negative values of the CC in the ensemble mean mainly concentrate on the western ghats and northern parts of the Indian region, particularly over the Indo-Gangetic belt (Fig. 1c). To understand the reason for such high negative values in the ensemble mean, the bottom panel shows the ENSO–ISMR relationship for the individual ensemble members. It is worth noting that the response of ENSO to ISMR varies significantly among ensemble members, ranging from −0.37 to −0.62. Member 1 displays the weakest ENSO response to ISMR with a CC of −0.37. In contrast, other members show a considerably strong relationship, albeit weaker than the ensemble mean. In addition, the negative CC among the ensembles, particularly for members 2, 4, and 5, are heterogeneously clustered over northern India. As a result, when computing the ensemble average across members, the negative values are superimposed in such a way that enhances the ENSO–ISMR relationship in the ensemble mean compared to individual members.

To illustrate that the disparity in characteristics is not due to data subsampling, Fig. 2a shows the probability distribution of the ENSO–ISMR correlation coefficients. This distribution is generated through bootstrapping by randomly selecting 38 years from the 190 reforecast (38 years × five initial conditions). This process is randomized and repeated over 1000 times. Interestingly, the maximum likelihood of getting the correlation coefficient between ENSO–ISMR is −0.55 (i.e., the mode value), which closely aligns with the correlation observed for AM and observation (Fig. 1a). Furthermore, the ENSO–ISMR correlation of four out of the five ensemble members of model M1 is clustered around the mode value of the pdf. The probability of obtaining the correlation coefficient of the ensemble mean (CC = −0.7, indicated by the red diamond) is much lower than that of the CC computed using all

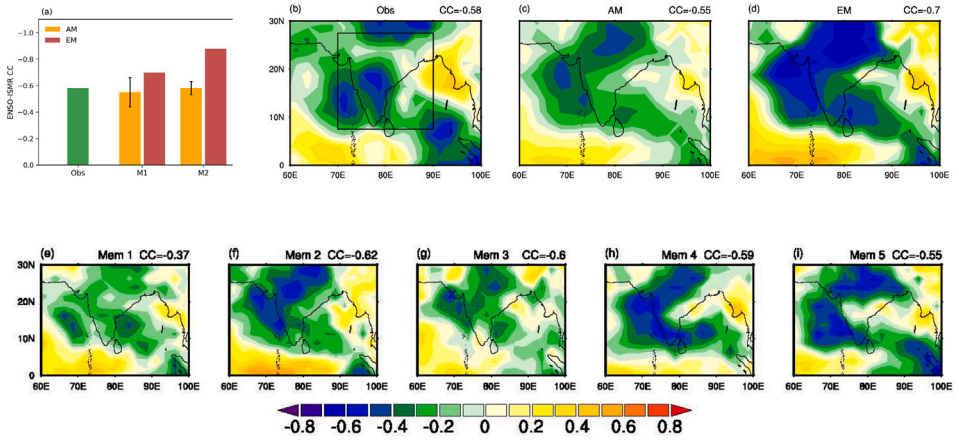

Fig. 1. (a) The bar plot illustrates the relationship between ENSO and ISMR for the observation, as well as the CFSv2 models M1 (with 5 ensemble members) and M2 (with 124 ensemble members). This relationship is depicted using both all ensemble members (AM) with 95% confidence band, and the ensemble mean (EM) of the CFSv2 seasonal hindcasts. Correlation coefficient (CC) values outside this interval are considered statistically significant. (b–h) The spatial distribution of the correlation coefficient between the ENSO index and precipitation over the South Asian region. Panel (b) represents the observation, panel (c) shows all member (AM), and (d) ensemble mean (EM), and panels (e–i) present the correlation for all five individual ensemble members of model M1 (21 April (Mem 1), 26 April (Mem 2), 1 May (Mem 3), 6 May (Mem 4), and 11 May (Mem 5)). The inset value in (b–h) is for the correlation coefficient (CC) between ISMR and ENSO index for 1979–2016.

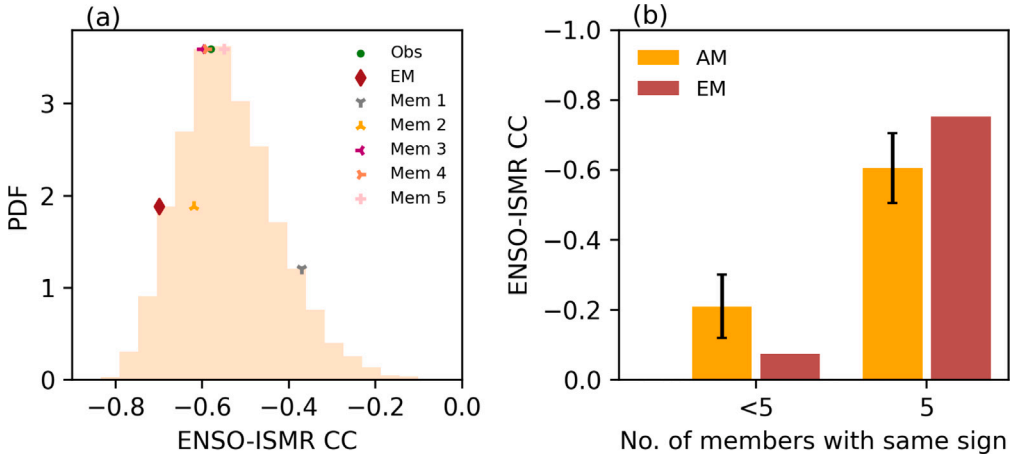

Fig. 2. (a) The probability density function (PDF) of the correlation coefficient (CC) between ENSO forcing and Indian summer monsoon rainfall (ISMR). This distribution is generated through bootstrapping by randomly selecting a 38-years from a total of 190 years of reforecast. This process is randomized and repeated over 1000 iterations. Additionally, the CC values for the observation, the ensemble mean, and all five individual ensemble members (21 April (Mem 1), 26 April (Mem 2), 1 May (Mem 3), 6 May (Mem 4), and 11 May (Mem 5)) for the period of 1979–2016 are also indicated as markers. (b) The bar plot shows the ENSO–ISMR relationship when all 5 and less than 5 ensemble members exhibit the same sign of ENSO anomalies for AM with 95% confidence band, and EM. Correlation coefficient (CC) values outside this interval are considered statistically significant. The year distribution of the cases where there are 5 and <5 members having the same sign of ENSO anomalies are shown in Fig. 3.

ensemble members, AM (CC = −0.55). This confirms that the ENSO–ISMR characteristics differ significantly between the EM and AM cases, and this discrepancy is not a result of data subsampling.

To investigate the cause of the differing response of the ENSO monsoon relationship between the ensemble mean (EM) and all members together (AM), we generate a histogram illustrating the nature of the ENSO forcing (i.e., the sign of the area-averaged SST anomalies over the Niño 3.4 region) across various ensemble members of the model M1, as shown in Fig. 3a. Our analysis shows that there is a high probability (around 66%) of obtaining the same sign of Niño 3.4 3.4 SST anomaly (either Niño 3.4 > 0 or Niño 3.4 < 0) for a given season across all ensemble members. This substantially strengthens and retains the ENSO signal in the ensemble mean, resulting in a robust ENSO–ISMR relationship in the ensemble mean. This is demonstrated by a strong correlation coefficient of −0.77 among the members displaying coherent signs of the ENSO forcing, as shown in Fig. 2b. On the contrary, the influence of members exhibiting incoherent signs of Niño 3.4 SST anomaly (<5) is minimal ($CC_{<5}$ = −0.08, Fig. 2b). Hence, their contribution to the ensemble mean is also insignificant. This suggests that the strong ENSO–ISMR relationship in the ensemble mean of the CFSv2 model is primarily governed by the greater number of ensemble members exhibiting the same sign of ENSO signal for a given season.

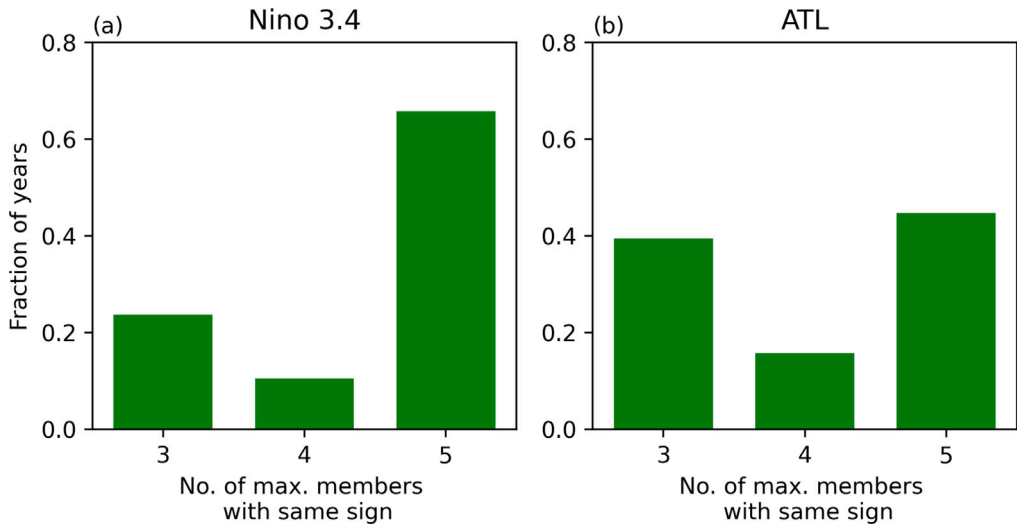

Fig. 3. The histograms show the distribution of the maximum number of ensemble members exhibiting the same signs of an SST anomaly for (a) ENSO Index (Niño 3.4) and (b) Atlantic tropical variability Index (ATL).

Furthermore, we perform the same analysis for all ensemble members together instead of performing the ensemble mean. We find that the ENSO–ISMR relationship for incoherent members (<5) is weaker for the ensemble mean compared to when all members are considered. Conversely, this is not observed in the case of coherent members. This could be attributed to the offsetting effects of the varying responses of ENSO among different ensemble members for the <5 case. Conversely, when considering non-ENSO forcing, such as ATL, the probability of all five ensemble members showing the same sign is considerably lower compared to the ENSO forcing (Fig. 3b). This discrepancy may be attributed to nonlinear processes occurring over the Atlantic Ocean in the model, leading to varying behaviors among ensembles. Thus, in the case of non-ENSO forcing, despite its presence in individual members, it demonstrates considerable variability, leading to the attenuation of non-ENSO signals in the ensemble mean.

Tropical climatic events, such as ENSO and ATL, tend to perturb the surface pressure patterns surrounding the Indian region, leading to changes in the incoming and outgoing moisture fluxes (Chakraborty and Singhai, 2021). These fluxes, primarily from the Arabian Sea (F_W) and the Bay of Bengal (F_E), play a vital role in driving atmospheric convection over India during the boreal summer monsoon season. Fig. 4 shows a scatter plot highlighting the difference in the response of ENSO and ATL forcing to moisture fluxes among members exhibiting coherent and incoherent (<5) signs of forcing (similar to Fig. 3). Here, we focus on dominant moisture fluxes such as F_E, which is crucial in regulating ENSO-driven rainfall in the CFSv2 model (Supplementary Figures 2a and 2b, also shown by Singhai et al. (2023). Similarly, F_W plays a dominant role in driving rainfall during ATL events (Supplementary Figures 2c and 2d). We observe that the correlation between ENSO and F_E is higher in years when all members exhibit a coherent sign of ENSO (CC = 0.84) compared to those with incoherent sign members (CC = 0.42). Hence, the impact of F_E on the ensemble mean is stronger when all members exhibit coherent signs, while its influence diminishes for incoherent sign members. Moreover, as depicted in Fig. 4b, it is evident that the variability of ENSO forcing is significantly reduced in the case of incoherent sign members than members with coherent signs. It is due to the incoherent signs of ENSO forcing in the individual ensemble members, which counterbalance each other, leading to reduced variability of the ENSO signal. However, the impact of ENSO on F_W is weaker for both coherent and incoherent sign members (Supplementary Figure 3).

As depicted in Fig. 3b, the number of members with coherent signs is lower for ATL than for ENSO. As a result, the impact of ATL in the ensemble mean is reduced compared to ENSO. This reduction in ATL forcing leads to a weaker response, as shown in Fig. 4c and 4d. The impact of ATL on F_E is greater for coherent sign members than for incoherent ones, but it is weaker than the impact on F_W (Supplementary Figure 4). Moreover, similar to ENSO, the impact of ATL forcing on F_W is more pronounced when all members have the same anomaly sign, as opposed to incoherent sign members. This emphasizes that disparity in the impact of ENSO and ATL forcing on moisture fluxes between the ensemble mean and all ensemble members is primarily influenced by the number of ensemble members exhibiting coherent forcing signs.

Fig. 5 illustrates the response of rainfall to positive and negative phases of ENSO and ATL for both ensemble mean and all ensemble members together. The relationship between El Niño (La Niña) events and ISMR is observed to be different in the ensemble mean compared to all members. In the ensemble mean, nearly all El Niño (La Niña) events lead to a decrease (increase) in ISMR. However, this behavior is not observed when all members are taken into account, which is similar to observation. Hence, the model accurately simulates the response of positive and negative ENSO phases to ISMR when considering all members compared to the ensemble mean. This difference is attributed to the strong ENSO–ISMR relationship observed in the ensemble mean, which results from a higher number of members exhibiting the coherent sign (as shown in Fig. 3a), thereby amplifying the ENSO signal in the ensemble mean. Conversely, similar to ENSO events, the rainfall variability sharply decreases in the ensemble mean compared to all ensemble members during ATL events. This could be attributed to the suppressed effect of ATL forcing due to the negation of the ATL signal caused by members having opposite anomaly signs.

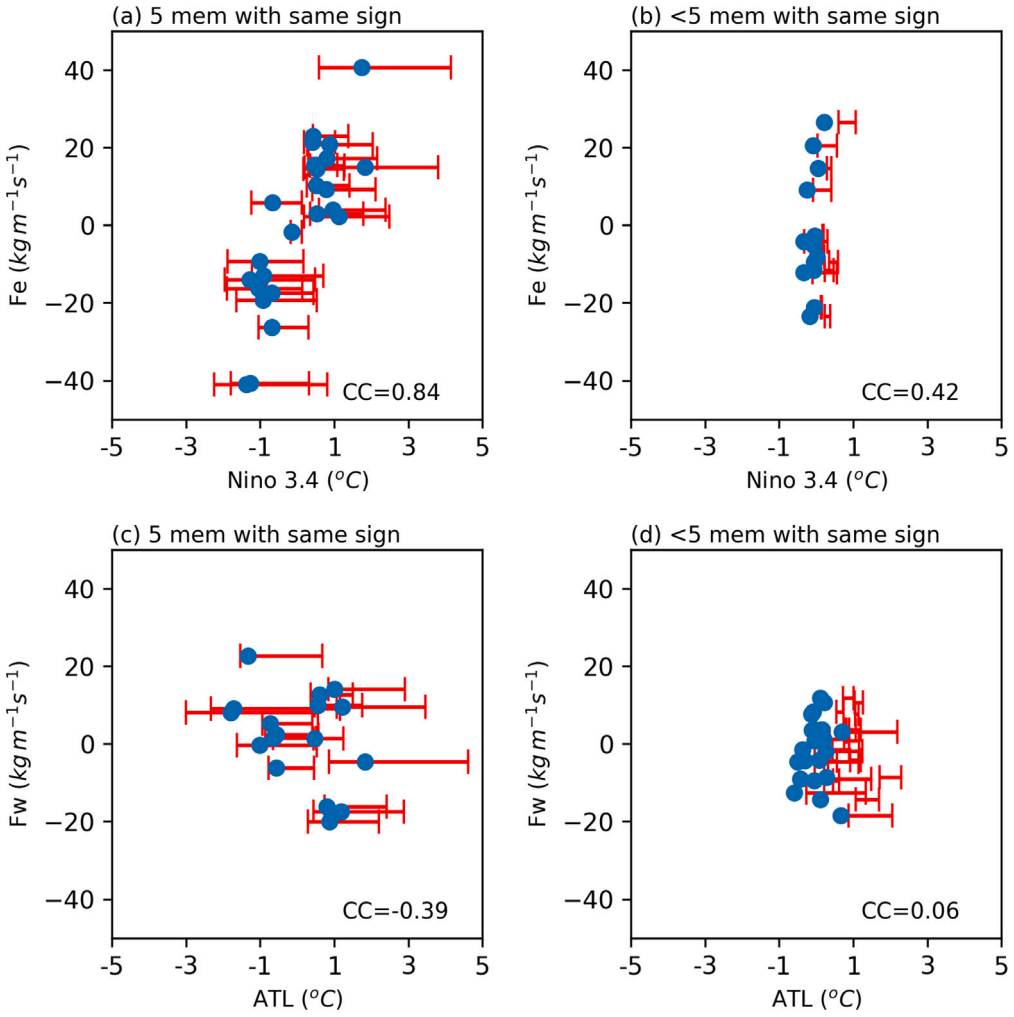

Fig. 4. The scatter plots show the relationship between the ENSO index and moisture flux over the Bay of Bengal (F_E) when there is a maximum of (a) five and (b) less than five ensemble members with the same signs of ENSO anomaly. Similarly, in plots (c, d), we examine the relationship between ATL index and moisture flux over the Arabian Sea (F_W) for these two cases. The whiskers denote the extreme values of the ENSO and ATL anomalies. To quantify the impact of ATL, we regress out the impact of ENSO from total moisture fluxes (explained in Supplementary Note 1).

4. Summary and discussions

Previous research has noted that the CFSv2 model, like many other climate forecast models, is subject to the strong influence of ENSO on ISMR (Kim et al., 2012; Shukla and Huang, 2016; He et al., 2022; Rajendran et al., 2021). Given this observation, it raises the question of why El Niño-related droughts in the CFSv2 are limited to one-third, whereas they account for two-thirds in observations (Singhai et al., 2023). Since numerous previous studies employ an ensemble mean approach to analyze ISMR teleconnection patterns, this method could neglect valuable information, such as inherent variability embedded within individual ensemble members. This could result in an overestimation of the model's teleconnection patterns. Therefore, in this study, we aim to investigate whether employing the ensemble mean approach accurately portrays the model's ability to simulate ISMR teleconnection patterns. Instead of analyzing individual ensemble members separately, we have chosen to evaluate all ensemble members together to represent the model's actual behavior in capturing the ENSO and ISMR relationship. Our analysis suggests that such a strong ENSO–ISMR relationship is primarily identified in the ensemble mean, which is not apparent when all ensemble members are taken into account. Hence, we aim to discern the underlying mechanisms contributing to the differing response of ENSO to ISMR in the ensemble mean compared to all ensemble members together.

This difference in the ENSO–ISMR relationship between the ensemble mean and all ensemble members is attributed to a change in the variability of SST forcing and its response to ISMR between ensemble members. In CFSv2, a higher number of ensemble members concur on the sign of the predicted ENSO signal for a particular season, thereby enhancing the ENSO signal and its associated ISMR response in the ensemble mean. Despite non-ENSO climate forcing being present in the individual ensemble members, it shows significant variability among them, leading to the suppression of the signal in the ensemble mean.

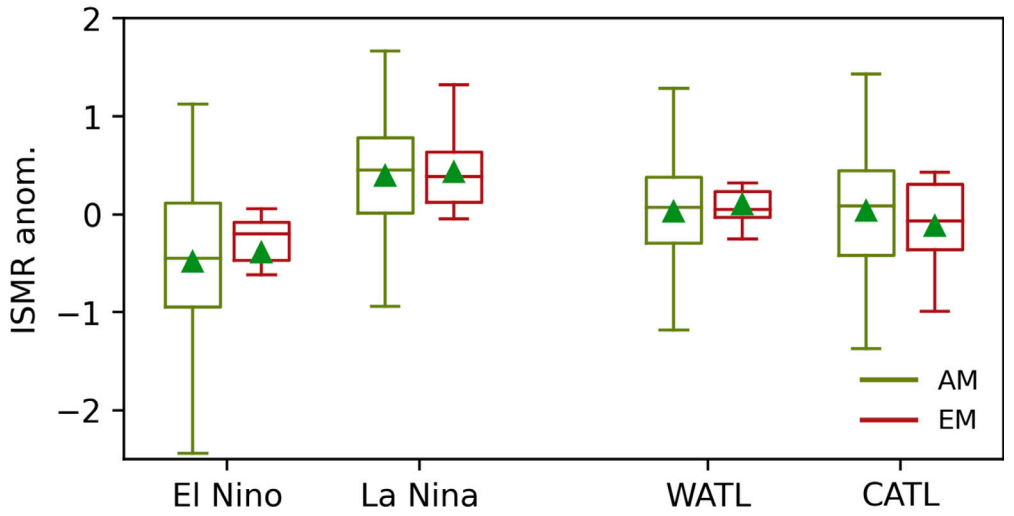

Fig. 5. The box plot shows the ISMR response to positive and negative phases of ENSO (El Niño and La Niña) and ATL (Warm-ATL and Cold ATL) forcing for all members (AM, green) ensemble mean (EM, red). The horizontal middle lines in the box plot indicate the median values. The box shows the interquartile range. The whiskers and triangle denote extreme and mean values, respectively.

In this study, we have not extended our findings to evaluate the role of ENSO in governing the year-to-year variation of other atmospheric phenomena in the CFSv2 model. However, a preliminary set of analyses (Supplementary Fig 5) investigating the difference in the role of ENSO in modulating West African summer monsoon rainfall (WASM) between the ensemble mean and all ensemble members confirms the findings above. Here, EM underestimates the ENSO–WASM relationship (CC = −0.42) compared to observations (CC = −0.5), unlike the ENSO–ISMR case where EM overestimates the relationship. Furthermore, the AM value (CC = −0.33) is weaker than EM, similar to the ENSO–ISMR relationship. Our theory holds good for seasonal predictions as the ensemble members are likely to be close together in representing the climate. It does not work, for example, in free runs of coupled models, as phases of ENSO (time of appearance) do not match between runs.

Our study highlights the significance of examining all ensemble members together to gain a comprehensive understanding of a model's behavior in simulating the teleconnection patterns rather than solely relying on the ensemble mean approach. Although the ensemble mean is used to identify the predictable signal in the climate system, it might not be the most suitable for diagnosing the model's characteristics. Here, we note the discrepancy in the ISMR teleconnection between the ensemble mean and all members observed within the CFSv2 model. However, this analysis has the potential to be expanded to investigate various physical processes in other climate models. We plan to address this in the subsequent study.

Code availability

NCL and Python codes are available upon request to the corresponding author.

CRediT authorship contribution statement

Priyanshi Singhai: Writing – original draft, Visualization, Validation, Methodology, Formal analysis, Conceptualization. **Arindam Chakraborty:** Writing – review & editing, Supervision, Conceptualization. **Kaushik Jana:** Writing – review & editing, Methodology. **Kavirajan Rajendran:** Writing – review & editing, Resources, Data curation. **Sajani Surendran:** Writing – review & editing, Resources. **Kathy Pegion:** Writing – review & editing, Supervision.

Declaration of competing interest

The authors declare that they have no known competing financial interests or personal relationships that could have appeared to influence the work reported in this paper.

Acknowledgments

AC, KR, and SS acknowledge NMM MoES GoVt India for supporting the research. AC also acknowledges support from DST's Centre for Climate Change at the Divecha Centre for Climate Change. The authors thank IMD and NCEP for providing rainfall and atmospheric data sets.

Appendix A. Supplementary data

Supplementary material related to this article can be found online at https://doi.org/10.1016/j.dynatmoce.2024.101504.

Data availability

Data will be made available on request.

References

Ashok, K., Guan, Z., Yamagata, T., 2001. Impact of the Indian ocean dipole on the relationship between the Indian monsoon rainfall and ENSO. Geophys. Res. Lett. 28 (23), 4499–4502.

Attada, R., Ehsan, M.A., Pillai, P.A., 2022. Evaluation of potential predictability of indian summer monsoon rainfall in ECMWF's fifth-generation seasonal forecast system (SEAS5). Pure Appl. Geophys. 179 (12), 4639–4655.

Behera, S., Krishnan, R., Yamagata, T., 1999. Unusual ocean-atmosphere conditions in the tropical Indian Ocean during 1994. Geophys. Res. Lett. 26 (19), 3001–3004.

Casanova, S., Ahrens, B., 2009. On the weighting of multimodel ensembles in seasonal and short-range weather forecasting. Mon. Weather Rev. 137 (11), 3811–3822.

Cash, B.A., Kinter, III, J.L., Adams, J., Altshuler, E., Huang, B., Jin, E.K., Manganello, J., Marx, L., Jung, T., 2015. Regional structure of the Indian summer monsoon in observations, reanalysis, and simulation. J. Clim. 28 (5), 1824–1841.

Chakraborty, A., Singhai, P., 2021. Asymmetric response of the Indian summer monsoon to positive and negative phases of major tropical climate patterns. Sci. Rep. 11 (1), 1–13.

Charney, J.G., Shukla, J., 1981. Predictability of monsoons. Monsoon Dyn. 99–110.

Chattopadhyay, R., Rao, S.A., Sabeerali, C., George, G., Rao, D.N., Dhakate, A., Salunke, K., 2016. Large-scale teleconnection patterns of Indian summer monsoon as revealed by CFSv2 retrospective seasonal forecast runs. Int. J. Climatol. 36 (9), 3297–3313.

Christiansen, B., 2018. Ensemble averaging and the curse of dimensionality. J. Clim. 31 (4), 1587–1596.

Christiansen, B., 2019. Analysis of ensemble mean forecasts: The blessings of high dimensionality. Mon. Weather Rev. 147 (5), 1699–1712.

Das, R.S., Rao, S.A., Pillai, P.A., Srivastava, A., Pradhan, M., Ramu, D.A., 2022. Why coupled general circulation models overestimate the ENSO and Indian Summer Monsoon Rainfall (ISMR) relationship? Clim. Dyn. 59 (9–10), 2995–3011.

Du, J., Mullen, S.L., Sanders, F., 1997. Short-range ensemble forecasting of quantitative precipitation. Mon. Weather Rev. (ISSN: 1520-0493) 125 (10), 2427–2459.

Ebert, E.E., 2001. Ability of a poor man's ensemble to predict the probability and distribution of precipitation. Mon. Weather Rev. (ISSN: 1520-0493) 129 (10), 2461–2480. http://dx.doi.org/10.1175/1520-0493(2001)129<2461:aoapms>2.0.co;2.

Ehsan, M.A., Singh, B., 2023. Forecast skill of Bangladesh summer monsoon rainfall in C3S and NMME models after calibration. Dyn. Atmos. Oceans 104, 101410.

Ehsan, M.A., Tippett, M.K., Robertson, A.W., Singh, B., Rahman, M.A., 2023. The ENSO fingerprint on Bangladesh summer monsoon rainfall. Earth Syst. Environ. 7 (3), 617–627.

Flato, G., Marotzke, J., Abiodun, B., Braconnot, P., Chou, S.C., Collins, W., Cox, P., Driouech, F., Emori, S., Eyring, V., et al., 2014. Evaluation of climate models. In: Climate Change 2013: The Physical Science Basis. Contribution of Working Group I To the Fifth Assessment Report of the Intergovernmental Panel on Climate Change. Cambridge University Press, pp. 741–866.

George, G., Rao, D.N., Sabeerali, C., Srivastava, A., Rao, S.A., 2016. Indian summer monsoon prediction and simulation in CFSv2 coupled model. Atmospheric Sci. Lett. 17 (1), 57–64.

Gleckler, P.J., Taylor, K.E., Doutriaux, C., 2008. Performance metrics for climate models. J. Geophys. Res.: Atmos. 113 (D6).

Hagedorn, R., Doblas-Reyes, F.J., Palmer, T.N., 2005. The rationale behind the success of multi-model ensembles in seasonal forecasting—I. Basic concept. Tellus A 57 (3), 219–233.

Hamill, T.M., Colucci, S.J., 1997. Verification of Eta–RSM short-range ensemble forecasts. Mon. Weather Rev. (ISSN: 1520-0493) 125 (6), 1312–1327.

He, L., Zhou, T., Chen, X., 2022. South Asian summer rainfall from CMIP3 to CMIP6 models: biases and improvements. Clim. Dyn. 1–13.

Huang, B., Thorne, P.W., Banzon, V.F., Boyer, T., Chepurin, G., Lawrimore, J.H., Menne, M.J., Smith, T.M., Vose, R.S., Zhang, H.M., 2017. NOAA extended reconstructed sea surface temperature (ERSST), version 5. NOAA Natl. Centers Environ. Inf. 30, 8179–8205.

Huffman, G.J., Adler, R.F., Bolvin, D.T., Gu, G., 2009. Improving the global precipitation record: GPCP version 2.1. Geophys. Res. Lett. 36 (17).

Kim, H.M., Webster, P.J., Curry, J.A., Toma, V.E., 2012. Asian summer monsoon prediction in ECMWF System 4 and NCEP CFSv2 retrospective seasonal forecasts. Clim. Dyn. 39, 2975–2991.

Krishnamurthy, V., 2018. Seasonal prediction of South Asian monsoon in CFSv2. Clim. Dyn. 51 (4), 1427–1448.

Krishnamurti, T., Kishtawal, C.M., LaRow, T.E., Bachiochi, D.R., Zhang, Z., Williford, C.E., Gadgil, S., Surendran, S., 1999. Improved weather and seasonal climate forecasts from multimodel superensemble. Science 285 (5433), 1548–1550.

Kucharski, F., Bracco, A., Yoo, J., Molteni, F., 2007. Low-frequency variability of the Indian monsoon–ENSO relationship and the tropical Atlantic: The "weakening" of the 1980s and 1990s. J. Clim. 20 (16), 4255–4266.

Kucharski, F., Bracco, A., Yoo, J., Molteni, F., 2008. Atlantic forced component of the Indian monsoon interannual variability. Geophys. Res. Lett. 35 (4).

Leutbecher, M., Palmer, T.N., 2008. Ensemble forecasting. J. Comput. Phys. 227 (7), 3515–3539.

Molteni, F., Buizza, R., Palmer, T.N., Petroliagis, T., 1996. The ECMWF ensemble prediction system: Methodology and validation. Q. J. R. Meteorol. Soc. 122 (529), 73–119.

Palmer, T.N., 2000. Predicting uncertainty in forecasts of weather and climate. Rep. Progr. Phys. 63 (2), 71.

Parthasarathy, B., Munot, A., Kothawale, D., 1994. All-India monthly and seasonal rainfall series: 1871–1993. Theor. Appl. Climatol. 49 (4), 217–224.

Pillai, P.A., Rao, S.A., V. Gangadharan, K., Pradhan, M., Srivastava, A., Jain, D.K., 2022. Impact of reduced ENSO variability and amplitude on ISMR prediction in the long-lead forecasts of monsoon mission CFS. Int. J. Climatol. 42 (16), 9166–9181.

Rajeevan, M., Bhate, J., Kale, J., Lal, B., 2006. High resolution daily gridded rainfall data for the Indian region: Analysis of break and active monsoon spells. Current Sci. 296–306.

Rajendran, K., Surendran, S., Varghese, S.J., Chakraborty, A., 2021. Do seasonal forecasts of Indian summer monsoon rainfall show better skill with February initial conditions? Curr. Sci. (00113891) 120 (12).

Rajendran, K., Surendran, S., Varghese, S.J., Sathyanath, A., 2022. Simulation of Indian summer monsoon rainfall, interannual variability and teleconnections: evaluation of CMIP6 models. Clim. Dyn. 58 (9–10), 2693–2723.

Ramu, D.A., Chowdary, J.S., Ramakrishna, S., Kumar, O., 2018. Diversity in the representation of large-scale circulation associated with ENSO-Indian summer monsoon teleconnections in CMIP5 models. Theor. Appl. Climatol. 132, 465–478.

Rasmusson, E.M., Carpenter, T.H., 1983. The relationship between eastern equatorial Pacific sea surface temperatures and rainfall over India and Sri Lanka. Mon. Weather Rev. 111 (3), 517–528.
Sabeerali, C., Ajayamohan, R., Bangalath, H.K., Chen, N., 2019. Atlantic Zonal Mode: An emerging source of Indian summer monsoon variability in a warming world. Geophys. Res. Lett. 46 (8), 4460–4467.
Saha, S., Moorthi, S., Pan, H.L., Wu, X., Wang, J., Nadiga, S., Tripp, P., Kistler, R., Woollen, J., Behringer, D., et al., 2010. The NCEP climate forecast system reanalysis. Bull. Am. Meteorol. Soc. 91 (8), 1015–1058.
Saha, S., Moorthi, S., Wu, X., Wang, J., Nadiga, S., Tripp, P., Behringer, D., Hou, Y.T., Chuang, H.y., Iredell, M., et al., 2014. The NCEP climate forecast system version 2. J. Clim. 27 (6), 2185–2208.
Shukla, R.P., Huang, B., 2016. Mean state and interannual variability of the Indian summer monsoon simulation by NCEP CFSv2. Clim. Dyn. 46, 3845–3864.
Shukla, J., Wallace, J., 1983. Numerical simulation of the atmospheric response to equatorial Pacific sea surface temperature anomalies. J. Atmos. Sci. 40 (7), 1613–1630.
Sillmann, J., Kharin, V., Zhang, X., Zwiers, F., Bronaugh, D., 2013. Climate extremes indices in the CMIP5 multimodel ensemble: Part 1. Model evaluation in the present climate. J. Geophys. Res. Atmos. 118 (4), 1716–1733.
Singh, B., Cash, B., Kinter, III, J.L., 2019. Indian summer monsoon variability forecasts in the North American multimodel ensemble. Clim. Dyn. 53 (12), 7321–7334.
Singh, B., Ehsan, M.A., Robertson, A.W., 2024. Calibrated probabilistic sub-seasonal forecasting for Pakistan's monsoon rainfall in 2022. Clim. Dyn. 1–19.
Singhai, P., Balakrishnan, S., Rajagopal, E., Chakraborty, A., 2020. Phase inconsistency as a major source of error in NGFS forecast. Clim. Dyn. 54 (5), 2797–2814.
Singhai, P., Chakraborty, A., Rajendran, K., Surendran, S., 2023. Why is the Indian summer monsoon in CFSv2 hypersensitive to moisture exchange with the Pacific Ocean? Clim. Dyn. 1–17.
Surcel, M., Zawadzki, I., Yau, M., 2014. On the filtering properties of ensemble averaging for storm-scale precipitation forecasts. Mon. Weather Rev. 142 (3), 1093–1105.
Tippett, M.K., Trenary, L., DelSole, T., Pegion, K., L'Heureux, M.L., 2018. Sources of bias in the monthly CFSv2 forecast climatology. J. Appl. Meteorol. Climatol. 57 (5), 1111–1122.
Toth, Z., Kalnay, E., 1997. Ensemble forecasting at NCEP and the breeding method. Mon. Weather Rev. (ISSN: 1520-0493) 125 (12), 3297–3319.
Weisheimer, A., Palmer, T., Doblas-Reyes, F., 2011. Assessment of representations of model uncertainty in monthly and seasonal forecast ensembles. Geophys. Res. Lett. 38 (16).